We are IntechOpen, the world's leading publisher of Open Access books Built by scientists, for scientists

4,800
Open access books available

122,000
International authors and editors

135M
Downloads

Our authors are among the

154
Countries delivered to

TOP 1%
most cited scientists

12.2%
Contributors from top 500 universities

WEB OF SCIENCE™

Selection of our books indexed in the Book Citation Index in Web of Science™ Core Collection (BKCI)

Interested in publishing with us?
Contact book.department@intechopen.com

Numbers displayed above are based on latest data collected.
For more information visit www.intechopen.com

1

Alloy Steel: Properties and Use First-Principles Quantum Mechanical Approach to Stainless Steel Alloys

L. Vitos[1,2,3], H.L. Zhang[1], S. Lu[1], N. Al-Zoubi[1], B. Johansson[1,2], E. Nurmi[4], M. Ropo[4], M. P. J. Punkkinen[4] and K. Kokko[4]

[1]*KTH Royal Institute of Technology,*
[2]*Research Institute for Solid State Physics and Optics,*
[3]*Uppsala University,*
[4]*University of Turku,*
[1,3]*Sweden*
[2]*Hungary*
[4]*Finland*

1. Introduction

Accurate description of materials requires the most advanced atomic-scale techniques from both experimental and theoretical areas. In spite of the vast number of available techniques, however, the experimental study of the atomic-scale properties and phenomena even in simple solids is rather difficult. In steels the challenges become more complex due to the interplay between the structural, chemical and magnetic effects. On the other hand, advanced computational methods based on density functional theory ensure a proper platform for studying the fundamental properties of steel materials from first-principles. In 1980's the first-principles description of the thermodynamic properties of elemental iron was still on the borderline of atomistic simulations. Today the numerous application-oriented activities at the industrial and academic sectors are paired by a rapidly increasing scientific interest. This is reflected by the number of publications on *ab initio steel research*, which has increased from null to about one thousand within the last two decades. Our research group has a well established position in developing and applying computational codes for steel related applications. Using our *ab initio* tools, we have presented an insight to the electronic and magnetic structure, and micromechanical properties of austenite and ferrite stainless steel alloys. In the present contribution, we review the most important developments within the *ab initio quantum mechanics aided steel design* with special emphasis on the role of magnetism on the fundamental properties of alloy steels.

Steels are mainly composed of iron and carbon and special properties are reached by introducing additional alloying elements. Stainless steels are among the most important engineering materials. They are alloy steels containing more than 12 percent Cr. Chromium forms a passive oxide film on the surface, which makes these alloys resistant against corrosion in various chemical environments (Wranglén, 1985). The main building block of ferrite stainless steels is the Fe-Cr alloy having the ferromagnetic α-Fe structure. Austenitic

stainless steels form the largest sub-category of stainless steels and comprise a significant amount of Ni as well. At low temperature, these alloys exhibit a rich variety of magnetic structures as a function of chemical composition, ranging from ferromagnetic phase to spin-glass and antiferromagnetic alignments (Majumdar & Blanckenhagen, 1984). At ambient conditions, Ni changes the ferromagnetic α-Fe structure to the paramagnetic γ-Fe structure. Today austenitic stainless steels dominate the steels applications, where high corrosion resistance and excellent mechanical properties are required. The austenitic grades represent the primary choice also when nonmagnetic properties are concerned.

2. Fundamental properties

2.1 Mechanical properties

The behavior of materials under external load defines their mechanical properties. Deformations are usually described in terms of stress of force per unit area and strain or displacement per unit distance. Using the stress-strain relation one can distinguish elastic and plastic regimes (Aragon, Backer, McClintock, & al., 1966; Ghosh & Olson, 2002; Lung & March, 1999). At small stress, the displacement and applied force obey the Hooke's law and the specimen returns to its original shape upon unloading. Exceeding the so-called elastic limit, upon strain release the material is left with a permanent shape.

Within the elastic regime, the elastic constants play the primary role in describing the stress-strain relation, whereas in the plastic regime the mechanical hardness expresses the resistance of material to permanent deformations. Plastic deformations are facilitated by dislocation motion and can occur at stress levels far below those required for dislocation-free crystals. Mechanical hardness may be related to the yield stress separating the elastic and plastic regions, above which a substantial dislocation activity develops. In an ideal crystal dislocations can move easily because they only experience the weak periodic lattice potential. In real crystal, however, the movement of dislocation is impeded by obstacles, leading to an elevation of the yield strength. In particular, in solid solutions the yield stress is decomposed into the Peierls stress needed to move a dislocation in the crystal potential and the solid-solution strengthening contribution due to dislocation pinning by the randomly distributed solute atoms. The Peierls stress of pure metals is found to be approximately proportional to the shear modulus (Lung & March, 1999). Dislocation pinning by random obstacles is controlled by the size and elastic misfit parameters (Fleischer, 1963; Labusch, 1972; Nabarro, 1977). The misfit parameters, in turn, can be derived from the composition dependent elastic properties of bulk solids. The effect of alloying on the elastic moduli of Fe and Fe-based alloys was studied in several experiments (Ghosh & Olson, 2002; Speich, Schwoeble, & Leslie, 1972; Takeuchi, 1969). Many of those measurements, however, were performed on multiphase samples, and thus the obtained elastic parameters correspond to a mixed phase rather than to a well defined crystal structure and hence give no information about the solid-solution strengthening mechanism within a particular phase.

Besides the bulk parameters, the formation energies of two-dimensional defects are also important in describing the mechanical characteristics of solids. The surface energy, defined as the excess free energy of a free surface, is a key parameter in brittle fracture. According to Griffith theory (Lung & March, 1999), the fracture stress is proportional to the square root of

the surface energy, that is, the larger the surface energy is the larger the load could be before the solid starts to break apart. Another important planar defect is the stacking fault in close-packed lattices. In these structures, the dislocations may split into energetically more favorable partial dislocations having Burgers vectors smaller than a unit lattice translation. The partial dislocations are bound together and move as a unit across the slip plane. In the ribbon connecting the partials the original ideal stacking of close-packed lattice is faulted. The energy associated with this miss-packing is the stacking-fault energy (SFE). The equilibrium separation of the partial dislocations is determined by the balance of the repulsive interaction and the stacking fault energy. Generally, larger stacking fault energy corresponds to smaller distance between the partials. During the dislocation movement, the partials must re-combine in order to overcome the obstacles (e.g. solute atoms). The resistance of materials to plastic deformation decreases with increasing SFE and hence in order to increase their strength the SFE should be lowered. In solid-solutions, the stacking fault energy may be varied, whereby wider or narrower dislocations can be produced and the mechanical properties can be altered accordingly. In practice, SFE is controlled by alloying elements towards desired properties such as strength or work hardening rate. Although, the stacking fault energy in austenitic steels has been determined from experiments (Rhodes & Thompson, 1977; Schramm & Reed, 1975), it should be mentioned that it is difficult to measure precisely and large inaccuracies are associated with the available experimental values (Vitos, Korzhavyi, Nilsson, & Johansson, 2008).

The immediate use of the stacking fault energies in steel design is beyond doubt. However, studying the stacking faults in steel alloys has some fundamental aspects as well. The stacking fault energy, to a good approximation, is proportional to the Gibbs energy difference between the hexagonal close packed (hcp) and face centered cubic (fcc) phases (Ishida, 1976). In contrast to the fcc phase, the magnetic free energy vanishes in the hcp Fe (ε-Fe) indicating that the local moments disappear in this phase (Grimvall, 1976). Therefore, the stacking fault energy appears to be a perfect candidate for detecting the footprint of room-temperature spin fluctuations on the mechanical properties of austenitic steels. In Sections 4.1, 4.2 and 4.4, we review some of our results on the elastic properties and stacking fault energies of Fe-based alloys.

2.2 Surface properties

A metallic solid solution, consisting of components which are immiscible at low temperature, is thermodynamically unstable when quenched from high temperature and phase separation occurs during aging or annealing. The phase separation may take place through two different paths: nucleation and growth (NG) and spinodal decomposition (SD). NG is initiated by small nuclei with large compositional fluctuations relative to the host and occurs within the metastable region of the miscibility gap. SD, on the other hand, is characterized by extended domains with fluctuating compositions which develop both in size and compositions toward their equilibrium states during aging.

For both paths, the interfacial energy (γ_i) between the decomposed phases plays an important role. According to Gibbs theory (Gibbs, 1948), the extremum of the work required to form a heterogeneous spherical grain of radius R determines the critical nucleus size R_{crit}, which in turn depends on γ_i. A nucleus will grow continuously with initial size $R \geq R_{crit}$ and disappear with $R < R_{crit}$. For SD, the interfacial energy corresponds to the gradient energy

that determines the critical wave-length of the fluctuations as shown by the phenomenological models developed to describe the kinetics and thermodynamics of SD (Hillert, 1961).

Owing to the large miscibility gap below about 500 ^{o}C, Fe-Cr is a typical binary system showing phase decomposition. When aged at the temperature range of 300-500 ^{o}C, alloys with composition within the miscibility gap separates into α (Fe-rich) and α' (Cr-rich) phases, both having the body centered cubic (bcc) structure. The phenomenon is commonly known as the „475 ^{o}C embrittlement'' and it degrades seriously the alloy properties. Although tremendous efforts have been made to investigate the phase decomposition of Fe-Cr alloys, due to the complexity of the interface the accurate determination of the composition dependent interfacial energy, either experimentally or theoretically, has been very limited. Recently, we evaluated the interfacial energy between the α and α' phases of the Fe-Cr alloys and investigated the effect of chemistry and magnetism (Lu, Hu, Yang, Johansson, & Vitos, 2010). Our study provides an insight into the fundamental physics behind the phase decomposition which is not accessible by the phenomenological theories.

The corrosion rate of Fe-Cr alloys decreases drastically within a narrow concentration interval (9-13 wt. % Cr), (Khanna, 2002; Ryan, Williams, Chater, Hutton, & McPhail, 2002; Wranglén, 1985) making the transition from iron-type to non-corrosive behavior quite abrupt. During oxidation, first a monolayer of oxide is formed instantly on the clean alloy surface exposed to oxidizing environment. The type of the initial oxide layer depends on the oxygen pressure, temperature and the actual alloy compositions within the first few surface layers. High surface density of the chemically less active atoms may also initiate the internal oxidation of the active alloy components. Focusing on the surface phenomena, further oxidation assumes transport of metal and oxygen ions through the initially formed oxide film. The ion transport is controlled by diffusion, which in turn is determined by the defect structure of the oxide layer. The high mobility of Fe in Fe oxides, especially in FeO, which is the dominant oxide component on pure iron above 570 ^{o}C, explains the corrosive nature of Fe. The passivity in Fe-Cr, on the other hand, is attributed to a stable Cr-rich oxide scale. Above the critical concentration a pure chromia layer is formed which effectively blocks the ion diffusion across the oxide scale.

Describing the oxide layer growth and ultimately the passivity of stainless steels is an enormous task as it requires the knowledge of the thermodynamic and kinetic properties of the oxide as well as oxide-metal and oxide-gas interfaces under oxidizing conditions. Many times the kinetics of the oxidation process is so slow that the real thermodynamic equilibrium is never reached during the active lifetime of the alloy product. Today massive information is available about the properties of the oxide scale on Fe-Cr, but the initial stage of the oxidation is still unclear. This is due to the experimental difficulties connected to the timescale of the initial oxidation of clean alloy surfaces. Large number of models were put forward for the kinetics of the thin layer oxidation and oxide scale formation (Khanna, 2002). Most of these theories, however, left in the shadow the active role of the metallic substrate in the oxidation process, simplifying it to a cation and electron reservoir. This might be a justified approximation after a monolayer or a few layers of oxide are built up. Nevertheless, the atomic level behavior of the metallic Fe-Cr surfaces is indispensable for understanding the oxygen chemisorption and the initial thin layer oxide formation on this class of materials.

Numerous former first-principles calculations focused on the properties of the Fe-rich Fe-Cr surfaces (Geng, 2003; Nonas, Wildberger, Zeller, Dederichs, & Gyorffy, 1998; Ponomareva, Isaev, Skorodumova, Vekilov, & Abrikosov, 2007; Ruban, Skriver, & Nørskov, 1999). However, due to the involved approximations and constrains, most of these studies failed to reproduce the experimentally observed Cr enrichment on the alloy surface (Dowben, Grunze, & Wright, 1983). A few years ago, we demonstrated that the Fe-Cr surfaces exhibit a compositional threshold behavior (Ropo et al., 2007). In particular, we showed that about 9 at. % chromium in Fe-Cr induces a sharp transition from Cr-free surfaces to Cr-containing surfaces. This surprising surface behavior was found to be a consequence of the complex bulk and surface magnetic interactions characteristic to the Fe-Cr system. The predicted surface chemical threshold has recently been confirmed by an independent theoretical study by Kiejna and Wachowicz (Kiejna & Wachowicz, 2008).

In Section 4.3, we review our theoretical study of the interfacial energy between the α and α' phases of Fe-Cr alloys, and in Section 4.5 we discuss the surface and magnetic properties of the iron-rich Fe-Cr alloys.

3. Computational approach

Today there is a large number of first-principles computational tools available which can in principle be employed to study the fundamental properties of Fe-based systems. When it comes to the Fe-based solid solutions and especially to paramagnetic austenitic stainless steel alloys, the number of suitable first-principles tools is very limited. Our ability to reach an *ab initio* atomistic level approach in the case of such complex systems has become possible by the Exact Muffin-Tin Orbitals (EMTO) method (Andersen, Jepsen, & Krier, 1994; Vitos, 2001, 2007). This *ab initio* computation tool is an improved screened Korringa-Kohn-Rostoker method for solving the one-electron equations within density functional method (Hohenberg & Kohn, 1964). It is based on the Green's functional and full charge density techniques (Kollár, Vitos, & Skriver, 2000). The problem of disorder is treated within the coherent-potential approximation (CPA) (Györffy, 1972; Soven, 1967; Vitos, Abrikosov, & Johansson, 2001). The total charge density is obtained from self-consistent calculations based on the local density approximation for the exchange-correlation potential and the total energy is evaluated within the Perdew-Burke-Ernzerhof (PBE) generalized gradient approximation for the exchange-correlation functional (Perdew, Burke, & Ernzerhof, 1996). The paramagnetic state of various Fe alloys is simulated by the so-called disordered local moment (DLM) model (Györffy, Pindor, Stocks, Staunton, & Winter, 1985). Within the DLM picture, a paramagnetic $Fe_{1-x}M_x$ binary alloy is described as a quaternary $(Fe^{\uparrow}Fe^{\downarrow})_{1-x}(M^{\uparrow}M^{\downarrow})_x$ alloy, with the equal amount of spin up (↑) and spin down (↓) atoms. Thereby, even though formally our calculations are performed at 0 K, the effect of the loss of the net magnetic moment above the Curie temperature on the total energy is correctly captured.

The EMTO approach in combination with the CPA is an efficient tool for describing alloying effects on the atomic-scale properties of random substitutional solid solutions. Its particular strength is that it is suitable to study properties and processes involving anisotropic lattice distortions or low symmetry structures. Due to the employment of optimized overlapping muffin-tin potential approach and the single-site approximation, this method has some limitations for systems with substantial charge transfer between alloy components or when

the short range order and local lattice relaxation effects become important. To control the above problem, applications are often preceded by a series of test calculations to find the best numerical parameters for the problem in question.

4. Results and discussion

4.1 Elastic properties

Alloying plays a central role in designing advanced engineering materials with desired properties. Different solute atoms produce different effects on the fundamental properties of the host. In particular, the single-crystal and polycrystalline elastic parameters are amongst the basic intrinsic properties of materials. Understanding how the elasticity is affected by alloying provides important information on determining mechanical properties such as fracture, hardness, brittleness, plasticity *etc.* Due to the limited solubility, many of the experimental measurements of the elastic properties of Fe-based alloys (Ghosh & Olson, 2002; Speich et al., 1972; Takeuchi, 1969) were performed on multiphase samples, and thus the obtained elastic parameters correspond to a mixed phase rather than to a well-defined crystal structure and hence give no information about the solid-solution strengthening mechanism within a particular phase. The situation is even less satisfactory on the theoretical side.

4.1.1 Binary alloys

Iron is a major alloy component in modern industry due to its structural strength and high abundance. Bulk Fe is ferromagnetic (FM) with Curie temperature of 1043 K and crystallizes in the body-centered-cubic (bcc) structure. Above the Curie temperature, Fe adopts a paramagnetic (PM) bcc structure up to 1183 K. With increasing temperature, it transforms to face-centered-cubic phase (γ-Fe). At ambient pressure, paramagnetic γ-Fe is stable between 1183 K and 1667 K. Before the melting temperature of 1811 K, the paramagnetic bcc phase is stabilized again. Alloying makes the Fe phase diagram even more complex, since phase stability and magnetism are sensitive to alloying element, impurity concentration, and temperature. Different solute atoms may stabilize or destabilize the bcc or fcc phases. Here we quote some basic information regarding the binary Fe phase diagrams and the reader is referred to the multi-component phase diagrams for further details. Based on the experimental phase diagrams (Massalsk, 1986), the maximum solubility of Mn and Ni in α-Fe is 3 and 5.5 atomic percent (at.%), respectively. The bcc Fe-rich Fe-Al, Fe-Si, Fe-V, Fe-Cr, Fe-Co, and Fe-Rh alloys show solubility up to ~10 at. % impurity concentration. In the γ phase, the solubility limit of Al, Si, V, and Cr is about 1.3, 3.2, 1.4, and 11.9 at.%, respectively, whereas Fe-Mn, Fe-Co, Fe-Ni, and Fe-Rh form continuous solid solutions. Beyond these concentrations, the PM fcc Fe-Al, Fe-Si, Fe-V, and Fe-Cr alloys transform to PM bcc alloys (with relatively narrow fcc-bcc two phase fields).

The elastic properties of ferromagnetic bcc and paramagnetic fcc $Fe_{1-x}M_x$ (M=Al, Si, V, Cr, Mn, Co, Ni, and Rh; $0 \le x \le 0.1$) binary alloys have been investigated (H. L. Zhang, Johansson, & Vitos, 2009; H. L. Zhang, Punkkinen, Johansson, Hertzman, & Vitos, 2010a; H. L. Zhang, Punkkinen, Johansson, & Vitos, 2010) using the exact muffin-tin orbitals density functional method in combination with the coherent-potential approximation.

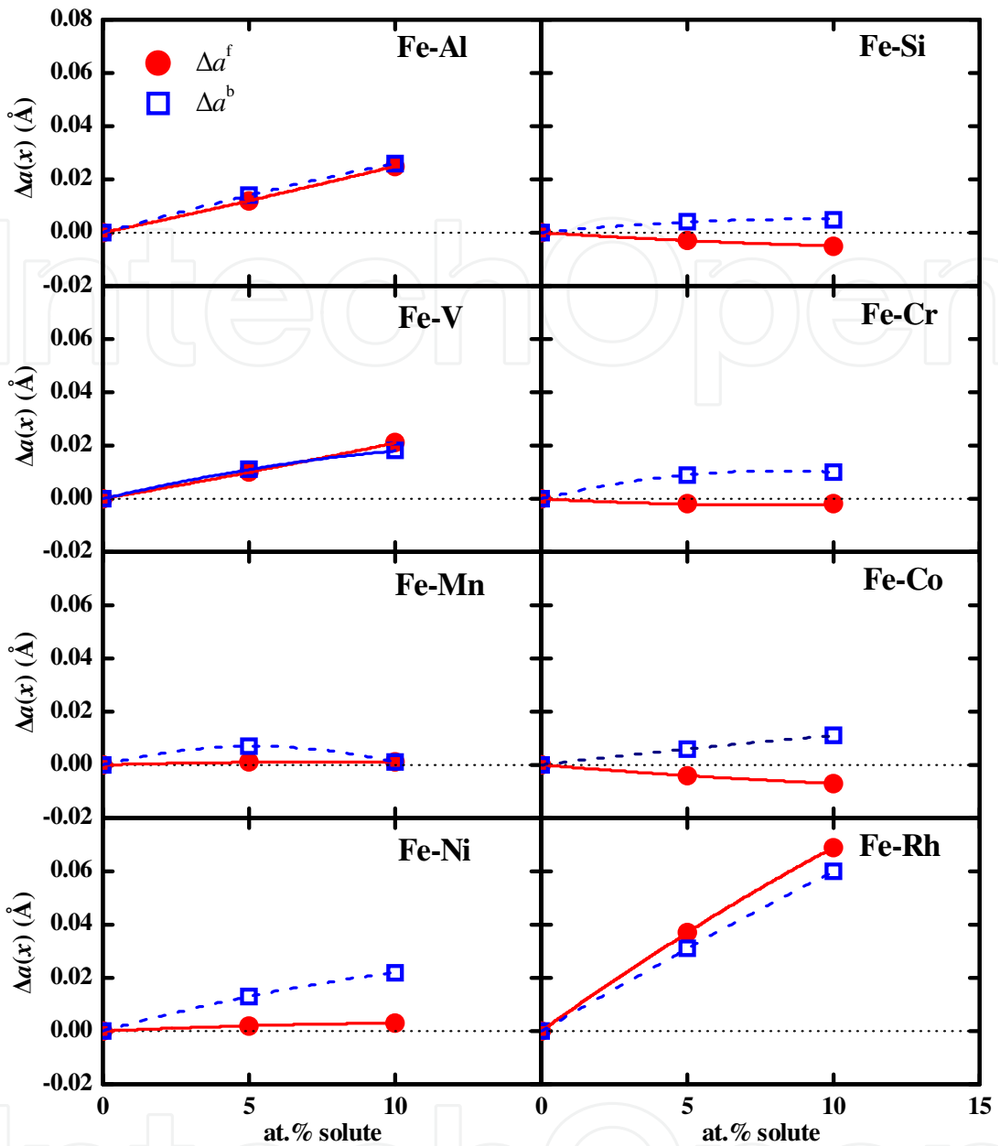

Fig. 1. Theoretical changes (relative to pure Fe) of the equilibrium lattice parameter $a(x)$ (in Å) for paramagnetic fcc (solid circles connected with solid lines) and ferromagnetic bcc (open squares connected with dashed lines) $Fe_{1-x}M_x$ (M=Al, Si, V, Cr, Mn, Co, Ni, and Rh; $0 \le x \le 0.1$) random alloys. The superscripts ^{f} and ^{b} denote the results for the fcc and bcc phases, respectively.

To calculate the elastic parameters of Fe-based alloys, first we computed the equilibrium lattice parameter for ferromagnetic bcc and paramagnetic fcc $Fe_{1-x}M_x$ (M=Al, Si, V, Cr, Mn, Co, Ni, and Rh; $0 \le x \le 0.1$) random alloys. To emphasize the alloying effect, in Fig. 1 we show the theoretical changes relative to pure Fe. We find that $a(x)$ of fcc Fe is strongly enlarged by Al, V, and Rh and slightly reduced by Si, Cr, and Co, while it remains nearly constant with Mn and Ni additions. Unlike the fcc phase, the calculated $a(x)$ of the bcc phase increases with alloying for all binaries considered here.

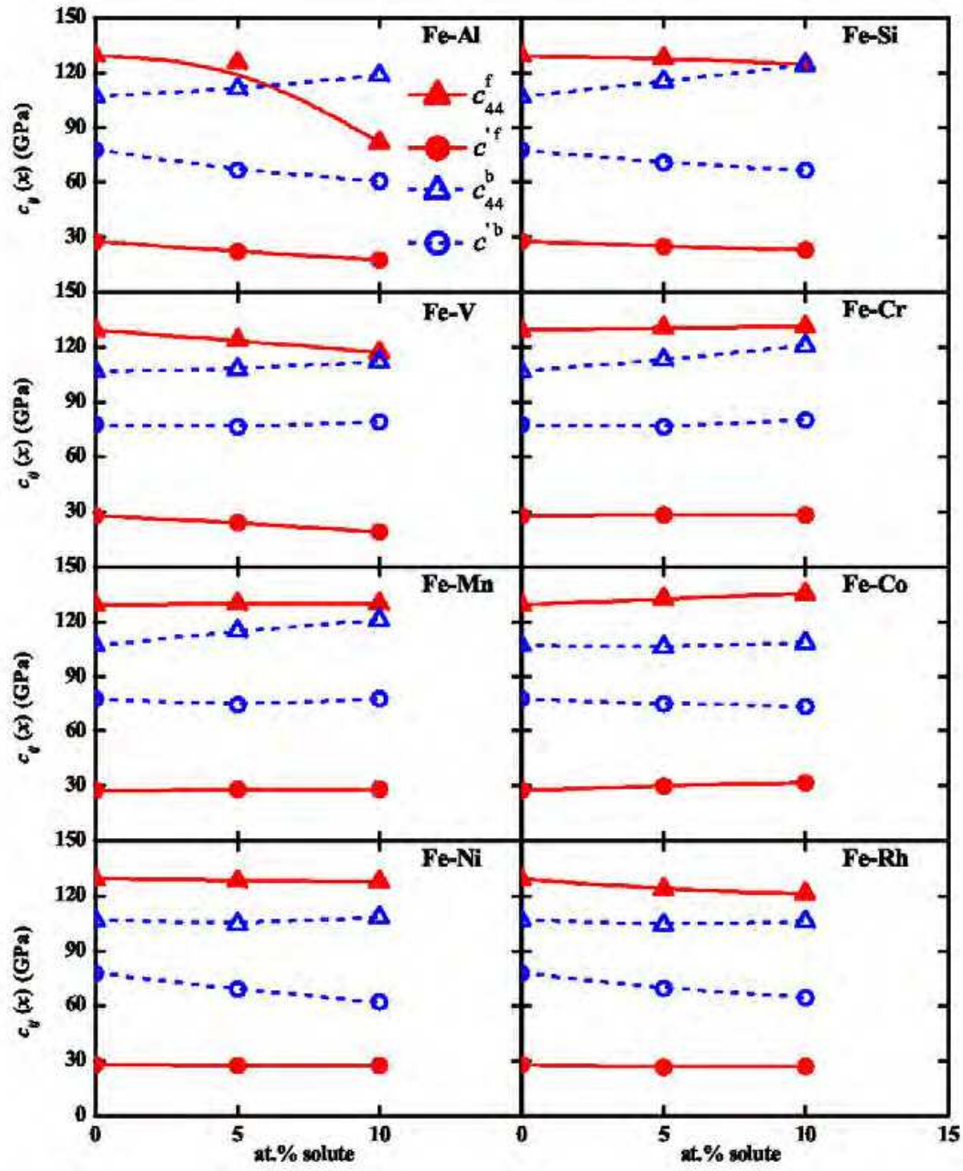

Fig. 2. Single-crystal shear elastic constants $c'(x)$ and $c_{44}(x)$ for paramagnetic fcc (solid symbols connected with solid lines) and ferromagnetic bcc (blue open symbols connected with dashed lines) $Fe_{1-x}M_x$ (M=Al, Si, V, Cr, Mn, Co, Ni, and Rh; $0 \le x \le 0.1$) random alloys. The superscripts ^{f} and ^{b} denote the fcc and bcc phases, respectively.

The elastic constants of paramagnetic fcc and ferromagnetic bcc $Fe_{1-x}M_x$ (M=Al, Si, V, Cr, Mn, Co, Ni, and Rh; $0 \le x \le 0.1$) random alloys are shown in Fig. 2. We find that the paramagnetic fcc alloys have smaller tetragonal elastic constant c' than the ferromagnetic bcc ones. Meantime, the c_{44} is larger for fcc alloys than for bcc ones, with exception of Fe-Al and Fe-Si at large impurity concentrations. On the average, the alloying effect on the c' and c_{44} is rather small for both fcc and bcc phases. The ferromagnetic bcc Fe-based alloys are

more isotropic than the paramagnetic fcc counterparts, and this difference to a large extent is due to the soft tetragonal mode (c') in the fcc phase.

With some exceptions, alloying has much larger effects on ferromagnetic bcc alloys than on paramagnetic fcc ones. However, in order to see where this stronger effect comes from, one should carry out similar calculations for the paramagnetic bcc Fe-based alloys to be able to exclude the effect of crystal lattice from the above comparison.

4.1.2 Ternary alloys

The elastic constants are intrinsic properties of a particular crystal structure and thus their alloying and magnetic state dependence may be weaker than that experienced, e.g., in the case of stacking fault energies (Section 4.4). Indeed, our former calculation (Vitos, Korzhavyi, & Johansson, 2002) for the polycrystalline elastic moduli (derived from single crystal elastic constants) of paramagnetic fcc Fe-Cr-Ni alloys show weak composition dependence (Fig. 3). Nevertheless, as we will show below, these bulk parameters also exhibit magnetic state dependence and mechanisms changing the local magnetic moments within the paramagnetic phase are expected to alter the elastic properties of Fe-Cr-Ni alloys.

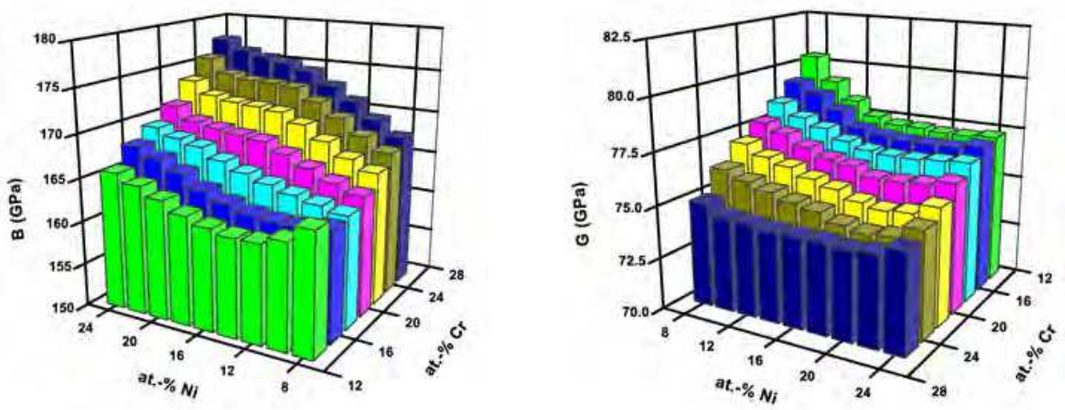

(a) (b)

Fig. 3. Calculated elastic parameters of austenitic stainless steels. The maps show the bulk modulus (a) and shear modulus (b) of paramagnetic Fe–Cr–Ni alloys as a function of the Cr and Ni concentrations (balance Fe).

We demonstrate the magnetic state dependence of the elastic constants of austenitic stainless steel alloys in the case of $Fe_{0.70}Cr_{0.15}Ni_{0.15}$ alloy by calculating the two single crystal shear elastic constants (c' and c_{44}) as a function of local magnetic moment on Fe sites (μ_{Fe}). The accuracy of our theoretical tool for this particular alloy was established previously (Vitos & Johansson, 2009). The theoretical equilibrium bulk parameters and the elastic constants for $Fe_{0.70}Cr_{0.15}Ni_{0.15}$ are compared with the available experimental data in Table 1. We find ~3.0% mean absolute relative deviation between the theoretical and experimental (Teklu et al., 2004) single-crystal elastic constants. As a matter of fact, this error is much smaller than that obtained for ferromagnetic bcc Fe (H. L. Zhang, Punkkinen, Johansson, Hertzman, & Vitos, 2010a). The conspicuously better accuracy achieved for Fe-Cr-Ni compared to Fe may

be ascribed to the fact that theory gives a highly accurate equation of state for paramagnetic Fe-Cr-Ni: the relative errors in the equilibrium atomic radius and bulk modulus being 0.4% and 1.1%, respectively.

	w_0	B	c_{11}	c_{12}	c'	c_{44}
theory	2.66	162.23	203.86	141.42	31.22	133.20
error	0.4	1.1	-2.5	4.0	-14.5	2.5
experiment	2.65	159-162	207-211	135-137	35-38	130

Table 1. Theoretical and experimental (Teklu et al., 2004) equilibrium Wigner-Seitz radius (w_0, in Bohr), bulk modulus (B, in GPa), and single-crystal elastic constants (c_{ij}, in GPa) of paramagnetic fcc $Fe_{0.70}Cr_{0.15}Ni_{0.15}$ alloy. The numbers from the second row are the relative deviations (in %) between the theoretical and the mean experimental values.

Figure 4a displays the c' and c_{44} elastic constants as a function of μ_{Fe} for spin-constrained calculations (solid lines) and for fully self-consistent calculations (single symbols at μ_{Fe} = 1.63 μ_B corresponding to the self-consistent result). The fact that the fully self-consistent and the spin-constrained results are relatively close to each other is due to the fact that upon lattice distortion the local magnetic moments do not change significantly. This is illustrated in Fig. 4b, where we plotted the local magnetic moment on Fe atoms for the paramagnetic $Fe_{0.80}Cr_{0.15}Ni_{0.05}$ alloy as a function of volume (Wigner-Seitz radius, w) and tetragonal lattice constant ratio c/a. The theoretical equilibrium w for the fcc phase is 2.66 Bohr, and for the body centred cubic (bcc) phase 2.68 Bohr. We recall that the fcc structure has $c/a \approx 1.41$ and the c' elastic constant is proportional with the curvature of the total energy versus c/a (for fixed volume). It is interesting to note that the local magnetic moments slightly increase upon tetragonal lattice distortion in the fcc phase (c/a≈1.41) and decrease in the bcc phase (c/a=1.0).

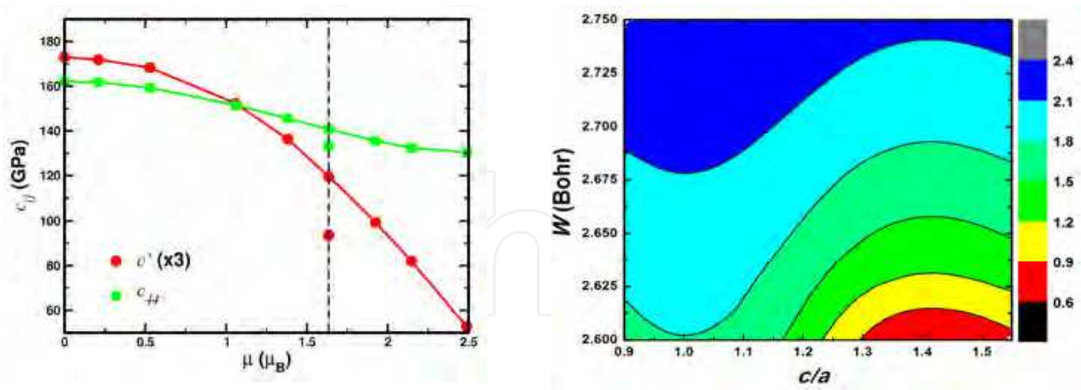

(a) (b)

Fig. 4. Left panel: Single-crystal elastic constants of paramagnetic fcc $Fe_{0.70}Cr_{0.15}Ni_{0.15}$ alloy as a function of the local magnetic moment on the Fe atoms. Note that c' has been multiplied by three in order to match its scale to that of c_{44}. Shown are also the floating-spin results obtained at the equilibrium magnetic moment μ_{Fe} = 1.63 μ_B (separate circle and square). All calculations were performed at paramagnetic volume (w=2.66 Bohr). Right panel: local magnetic moments on Fe atoms of paramagnetic $Fe_{0.80}Cr_{0.15}Ni_{0.05}$ alloy as a function of Wigner-Seitz radius w and tetragonal lattice parameter ratio c/a.

Returning to Fig. 4a, we observe that both elastic constants strongly depend on the local magnetic moment. The effect is somewhat more pronounced for the tetragonal elastic constant. From a polynomial fit to the data from Fig. 4a, for the slopes of the elastic constants versus magnetic moment we obtain $\delta c'/\delta\mu \approx -22.5$ GPa/μ_B and $\delta c_{44}/\delta\mu \approx -19.5$ GPa/μ_B. Hence, 0.1μ_B change in the local magnetic moment results in ~2 GPa change in the elastic constants, representing ~6% for c' and ~2% for c_{44}. This is an important effect, especially taking into account that we are dealing with a system well above its magnetic transition temperature. We suggest that by manipulating the magnetism, e.g., via chemical composition, chemical ordering, external field, or temperature, one is able to tailor the thermo-elastic properties of austenitic stainless steels. We have demonstrated the above effect in the case of the temperature dependence of the single crystal elastic constants of paramagnetic Fe-Cr-Ni alloys (Vitos & Johansson, 2009). In particular, we have shown that spin fluctuation in paramagnetic Fe-Cr-Ni alloys can account for 63% of $\delta c'/\delta T$ and 28% for $\delta c_{44}/\delta T$ as compared to the experimental measurements (Teklu et al., 2004).

4.2 Bain path

The transformation mechanism between the bcc and the fcc phases of Fe-based alloys is of key importance for the properties of alloy steels. This is a typical diffusionless structural change belonging to the group of the so called martensitic transformations. Several homogeneous paths have been suggested for describing the bcc-fcc transformation. In particular, the Bain path (Bain, 1924) is obtained by expanding the bcc lattice along one of the cubic axes (c) and contracting along the two others (a). Upon lattice deformation the crystal symmetry remains tetragonal and the unit cell is body centered tetragonal (bct). The tetragonality of the lattice is described by the c/a ratio. When c/a is 1 the bct lattice corresponds to the bcc one, whereas when c/a reaches $\sqrt{2}$ the bct lattice turns into the fcc one. The Bain path is an appropriate model for studying the energetics of the bcc-fcc martensitic transformation. Furthermore, monitoring the alloying induced softening or hardening of Fe-based alloys against tetragonal distortions (Al-Zoubi, Johansson, Nilson, & Vitos, 2011) is of key importance for understanding the interstitial driven martensitic transformations in alloy steels.

In Fig. 5, we present the calculated total energy maps for Fe-Cr and Fe-Cr-Ni alloys along with the Bain path. The energy map for $Fe_{0.90}Cr_{0.10}$ (Fig. 5a) shows that at the equilibrium volume the close-packed fcc structure is marginally more stable than the bcc modification, the energy differences between the fcc and the bcc structures being $\Delta E \equiv E_{fcc}-E_{bcc}$ = -0.021 mRy. There is a clear energy barrier, a saddle point between the bcc and fcc local minima. Approximating the energy barrier by the total energy calculated for c/a =1.2 and w = 2.675 Bohr, for $Fe_{0.9}Cr_{0.1}$ we obtain $\Delta E_f \equiv E_{1.2} - E_{fcc}$ = 1.019 mRy (barrier relative to the fcc structure) or $\Delta E_b \equiv E_{1.2} - E_{bcc}$ = 0.998 mRy (barrier relative to the bcc structure). Obviously $\Delta E_b - \Delta E_f = \Delta E$.

Since in the present calculations no temperature effects are taken into account (except the chemical and magnetic randomness in the total energy) the total energy difference ΔE between the fcc and bcc structures should be interpreted with precaution and should not be associated with the phase stability of Fe-Cr alloys. Nevertheless, we can make our conclusions more robust and identify the primary chemical effects on the phase stability by

considering the $Fe_{0.90}Cr_{0.10}$ as reference and focusing on the total energy of $Fe_{0.85}Cr_{0.1}M_{0.05}$ (M stands for Cr and Ni) expressed relative to that calculated for $Fe_{0.90}Cr_{0.10}$. The corresponding relative fcc-bcc energy difference is denoted by $\Delta E(M)$ and the relative energy barriers by $\Delta E_f(M)$ or $\Delta E_b(M)$. According to this definition, for instance vanishing $\Delta E(M)$ and $\Delta E_{f/b}(M)$ mean that 5 % alloying addition M produces negligible effect on the corresponding energy differences of $Fe_{0.9}Cr_{0.1}$.

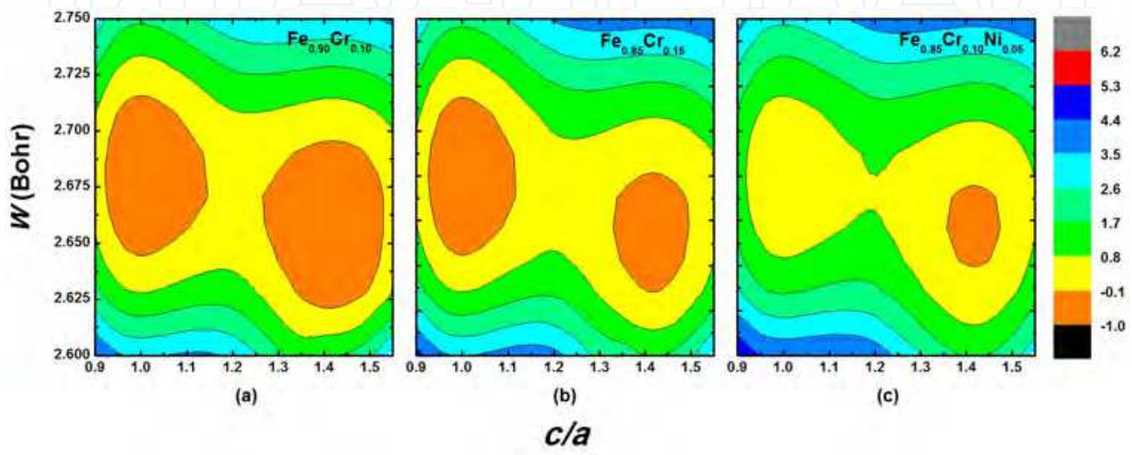

Fig. 5. Total energy contours (in mRy) for (a) $Fe_{0.9}Cr_{0.1}$, (b) $Fe_{0.85}Cr_{0.15}$ and (c) $Fe_{0.85}Cr_{0.1}Ni_{0.05}$ alloys as a function of the tetragonal lattice ratio (c/a) and the Wigner-Seitz radius (w). For each alloy, the energies are plotted relative to the minimum of the corresponding bcc (c/a = $(c/a)_{bcc}$ = 1) total energy.

Next, we illustrate the effect of adding 5% Cr and Ni on the Bain path of the paramagnetic Fe-Cr alloy. We find that adding 5 % Cr to the $Fe_{0.9}Cr_{0.1}$ alloy increases the fcc-bcc total energy difference by ΔE(Cr) = 0.443 mRy (Fig. 5b). In other words, the chemical effect of Cr is to stabilize the bcc phase relative to the fcc one. Alloying changes the energy barrier between the bcc and fcc structures as well. We obtain that 5 % Cr addition to $Fe_{0.9}Cr_{0.1}$ alters the barrier by ΔE_f(Cr) = -0.118 mRy or ΔE_b(Cr) = 0.325 mRy. That is, the energy minimum around the fcc phase becomes shallower and that around the bcc phase deeper by alloying with Cr. In terms of mechanical stability of alloys, the above alloying effect of Cr corresponds to mechanically less (more) stable fcc (bcc) phase. This is in line with the observation that Cr decreases the tetragonal elastic constant of paramagnetic fcc $Fe_{0.9}Cr_{0.1}$.

Nickel is calculated to have pronounced effects on the Bain path of paramagnetic Fe-Cr alloys (Fig. 5c). Adding 5 % Ni to $Fe_{0.9}Cr_{0.1}$ yields ΔE(Ni) = -0.300 mRy and changes the energy barrier by ΔE_f(Ni) = 0.045 mRy per atom or ΔE_b(Ni) = -0.255 mRy per atom relative to that of $Fe_{0.9}Cr_{0.1}$. It is interesting to contrast the above trends for the energy barrier with those calculated for the elastic constants of paramagnetic fcc Fe alloys (Section 4.1.1). In particular, Ni is calculated to decrease slightly the tetragonal elastic constant of fcc Fe. Thus we may conclude that the trends in the elastic constants are not sufficient to predict the changes in the fcc-bcc energy barrier upon alloying.

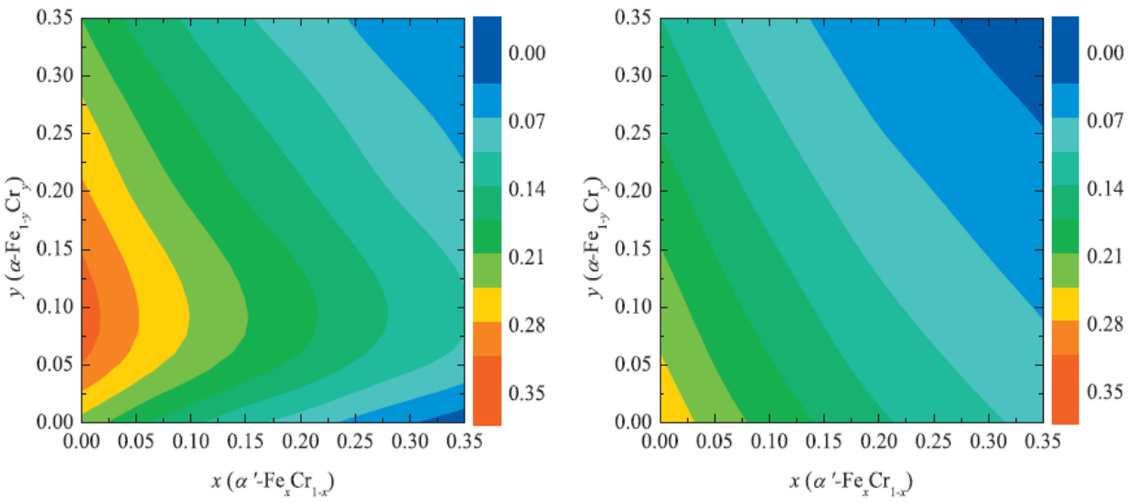

(a) (b)

Fig. 6. The (001) interfacial energy (in J m^{-2}) between the Cr-rich α' phase (Fe_xCr_{1-x}) and the Fe-rich α phase ($Fe_{1-y}Cr_y$) for (a) ferromagnetic and (b) paramagnetic states.

4.3 Interfacial energies

The interfacial energy (γ_i) between the two phases (Fe-rich α and Cr-rich α') in Fe-Cr alloys is an important parameter when studying the phase separation by spinodal or nucleation and growth mechanisms. While the experimental determination of the interfacial energy is less feasible, it can easily be evaluated by first-principles calculations. The (110) and (100) interfacial energies between the Fe-rich α-$Fe_{1-y}Cr_y$ and Cr-rich α'-Fe_xCr_{1-x} phases have been calculated (Lu et al., 2010) as a function of composition ($0<x, y<0.35$). It is found that generally the (110) interface has lower energy than the (001) one as expected from a simple bond-cutting model, and the interface energies vary in a similar way with respect to the composition. The interfacial energy for the (001) interface varies between 0.02 and 0.33 Jm^{-2} for the ferromagnetic state and between 0.02 and 0.27 Jm^{-2} for the paramagnetic state with respect to composition (Fig. 6.). The paramagnetic γ_i shows a monotonous decreasing trend with increasing x and y, while the ferromagnetic γ_i decreases with increasing x, but increases with y for $0<y<0.1$ and then decreases for $0.1<y<0.35$. The nonlinear concentration dependence of the ferromagnetic interfacial energy has been attributed to the complex magnetic interaction near the interface (Lu et al., 2010).

Using a continuum model, the critical grain size (R_{crit}) for phase separation may be estimated from the calculated interfacial energies (Fig. 7.). It is shown that the theoretical critical radius exhibits a strong dependence on the composition of the initial homogenous alloy. The critical radius is very small inside the spinodal line and increases significantly between the spinodal and solubility lines, which agrees well with the fact that in these two composition regions different mechanisms, spinodal or nucleus and growth, control the phase separation process.

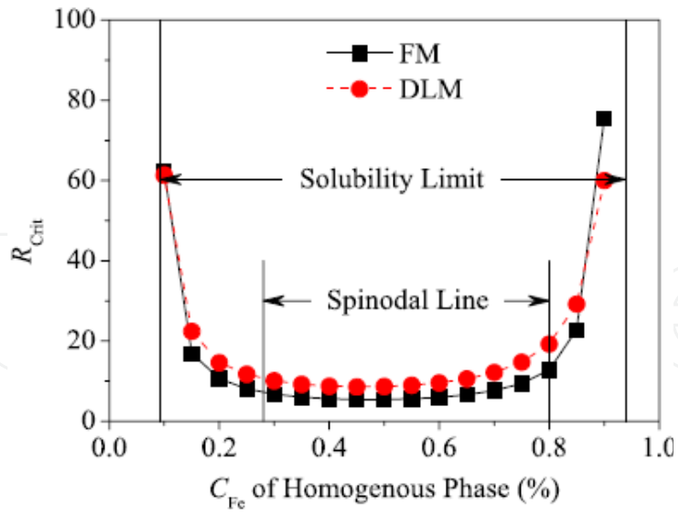

Fig. 7. Critical nucleus size (R_{crit} in Å) as a function of the composition of the homogenous phase Fe_cCr_{1-c} for ferromagnetic and paramagnetic states. The vertical lines show the experimental spinodal and solubility limits.

4.4 Stacking fault energies

The stacking fault energy of a material is an important characteristic since it is related to various mechanical properties such as strength, toughness and fracture *etc.* In austenitic stainless steels, SFE has been measured for various compositions (Rhodes & Thompson, 1977; Schramm & Reed, 1975). However, the experimental data show large scatter (Table 2) and thus the empirical relations between SFE and composition established based on such data cannot properly account for the correct alloying effects (Lo, Shek, & Lai, 2009).

Cr	Ni	theory	Experiment
15	14	40.1	46±7
17	13	30.9	23±5
17	20	38.8	31±5
19	10	11.7	7.2±1.5, 25±2.5, 16.4±1.1
22	13	18.4	18±4
26	20	42.0	40±5

Table 2. Comparison between the calculated and experimental (Vitos et al., 2008) stacking fault energies for six selected alloys. Compositions are given in atomic percent and SFE in mJ/m^2.

The SFE of Fe-Cr-Ni alloys have been calculated (Vitos, Korzhavyi, & Johansson, 2006; Vitos et al., 2008; Vitos, Nilsson, & Johansson, 2006) as a function of temperature and composition using the EMTO method (Fig. 8). These theoretical results reveal the underlying mechanisms determining the complicated relation between SFE and alloying elements. It is shown that the increasing effect of Ni on the SFE strongly depends on the content of Cr. In low Cr alloys, Ni has negligible effect on the SFE when the concentration of Ni is over ~12 at. %, while in high Cr alloys, the SFE is nearly linearly proportional to the amount of Ni. On

the other hand, Cr decreases the SFE only in low Ni alloys and in high Ni alloys the slope of SFE vs. Cr content changes sign at ~20 at. % Cr.

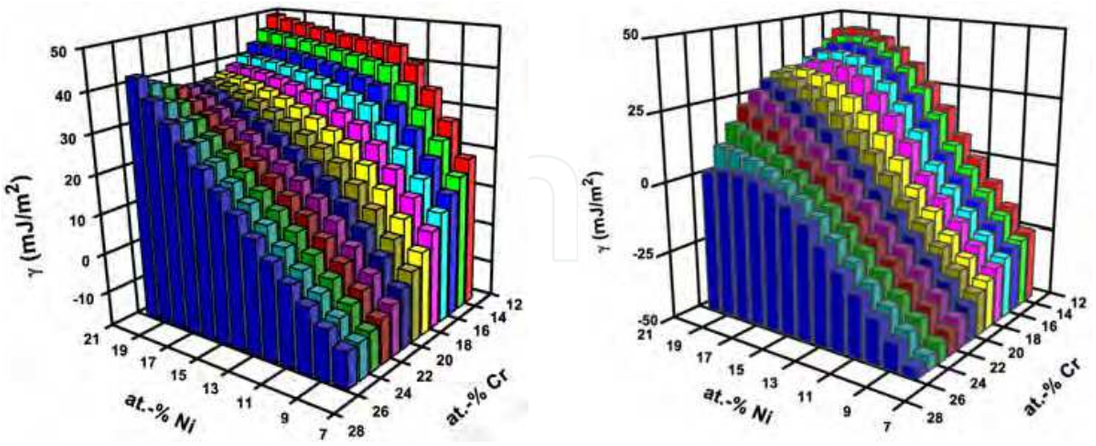

(a) (b)

Fig. 8. Calculated stacking fault energy (γ) of paramagnetic fcc Fe-Cr-Ni alloys plotted as a function of Ni and Cr contents for 300 K (left panel) and 0 K (right panel).

From Fig. 8a, one would conclude that in general with increasing Ni content in paramagnetic Fe-Cr-Ni alloys the width of the ribbon connecting the partial dislocations decreases so that the partials can more easily recombine and thus the resistance of the alloy against plastic deformation decreases. At the same time, Cr is predicted to enhance the strength of the alloy at low Ni content and have negligible effect at large Ni content. However, the above trends show strong temperature dependence. On the right panel of Fig. 8, we show the calculated SFE at 0 K. The overall effect of Ni at 0 K is similar to that from Fig. 8a, but Cr is found to decrease the SFE at any Ni content. We will show below that the reason behind this change is the behavior of the local magnetic moment with alloying.

We find that the above chemical effects of alloying additions are accompanied by major magnetic effects, which in fact stabilize the most common industrial alloy steels at normal service temperatures. Note that according to Fig. 8b, all Fe-Cr-Ni alloys encompassing less than ~11-17 % Ni (depending on Cr content) have negative SFE at 0 K. At 300 K, only alloys within a small compositional range have still negative SFE and they are located in the low-Ni-high-Cr part of the map from Fig. 8a. Within the present model, the temperature part of the SFE corresponds mainly to the magnetic entropy contribution to the SFE. Since the local magnetic moments in the double hexagonal structure are calculated to be close to those within the fcc structure, the magnetic fluctuation part of the SFE reduces to $\gamma^{mag} = -T[S^{hcp} - S^{fcc}]/A_{2D}$ (where S stands for the magnetic plus electronic entropy and A_{2D} is the interface area). γ^{mag} is plotted in Fig. 9a for 300 K. We can observe that γ^{mag} exhibits a strongly nonlinear composition dependence, especially for low-Ni alloys (as a function of Cr content) and for high-Cr alloys (as a function of Ni content). Because at 300 K the leading term in the entropy is the magnetic contribution, the above trends are direct consequences of the composition dependence of the magnetic moments for the fcc and hcp phases (Vitos, Nilsson et al., 2006).

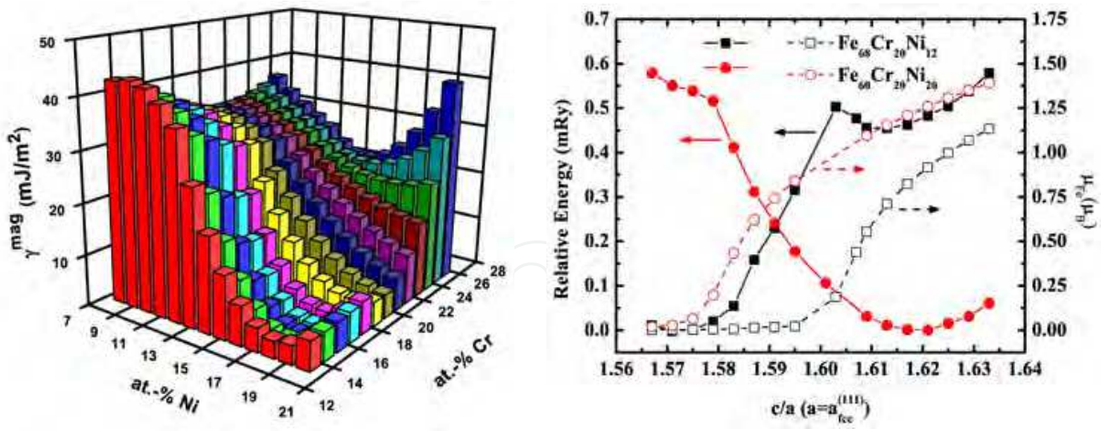

(a) (b)

Fig. 9. Left panel: magnetic fluctuation contribution to the stacking fault energy (γ^{mag}) of fcc Fe-Cr-Ni alloys calculated for 300 K. Right panel: total energy (left axis) and local magnetic moment (right axis) for the hcp Fe-Cr-Ni alloys as a function of hexagonal lattice parameter *c/a* keeping the in-plane lattice constant *a* fixed to that of the fcc lattice ($a_{fcc}^{(111)}$). Notice the different orientations of the Ni and Cr axes on Fig. 8 and Fig. 9a.

We illustrate the change of the local magnetic moments in the case of $Fe_{0.68}Cr_{0.20}Ni_{0.12}$ and $Fe_{0.60}Cr_{0.20}Ni_{0.20}$ alloys. According to the axial interaction model (Vitos, Nilsson et al., 2006), the stacking fault energy is computed from the total energies of the double hexagonal, hcp and fcc lattices. In these calculations, the atomic volume is assumed to be constant and equal to that of the parent fcc lattice. However, in real alloys due to the vanishing local magnetic moments in the hcp environment, the hcp lattice prefers a smaller equilibrium volume than that of the fcc lattice. Due to the in-plane lattice constraint volume relaxation can be realized only along the direction perpendicular to the stacking fault plane. To mimic this situation, in all our calculations we relaxed the *c* lattice constant of the hcp lattice while keeping the in-plane lattice constant *a* fixed to $a_{fcc}^{(111)}$ (Lu, Hu, Johansson, & Vitos, 2011). The calculated total energies are shown in Fig. 9b (left axis) as a function of *c/a*. In alloys containing 12 % Ni, the hexagonal lattice is nonmagnetic (the local magnetic moments vanish within the hcp phase, see Fig. 9b right axis) and thus there should be a large volume relaxation relative to the volume of the fcc lattice. This is reflected by the very small equilibrium $c/a \approx 1.57$ obtained for hcp $Fe_{0.68}Cr_{0.20}Ni_{0.12}$ and the large γ^{mag} calculated for this alloy (Fig. 9a). When the Ni content is increased to 20 %, the hcp lattice becomes weakly magnetic (small local magnetic moments appear on Fe sites, see Fig. 9b right axis). Therefore, the equilibrium volume of hcp $Fe_{0.60}Cr_{0.20}Ni_{0.20}$ should be close to that of the fcc phase. Indeed, the calculated equilibrium $c/a \approx 1.62$ for hcp $Fe_{0.60}Cr_{0.20}Ni_{0.20}$ is very close to the ideal one (~1.63), meaning that in this alloy no substantial volume relaxation takes place around the stacking fault. In consequence, the magnetic fluctuation contribution to the stacking fault energy of $Fe_{0.60}Cr_{0.20}Ni_{0.20}$ alloys becomes very small (Fig. 9a).

The results summarized in Figs. 8 and 9 clearly demonstrate the importance of the disordered local moments for the stacking fault energies of steels. For the magnetic contribution to the free energy one may employ models which are more advanced than the

mean-field approximation used here. However, this will not change the general conclusion that local magnetic moments have a marked contribution to the energetic of the stacking faults. Any mechanism (alloying, temperature or strong magnetic field) that can alter the magnetic structure of these alloys is predicted to have large impact on the stacking fault energies and thus on the strength of the paramagnetic Fe-Cr-Ni alloys.

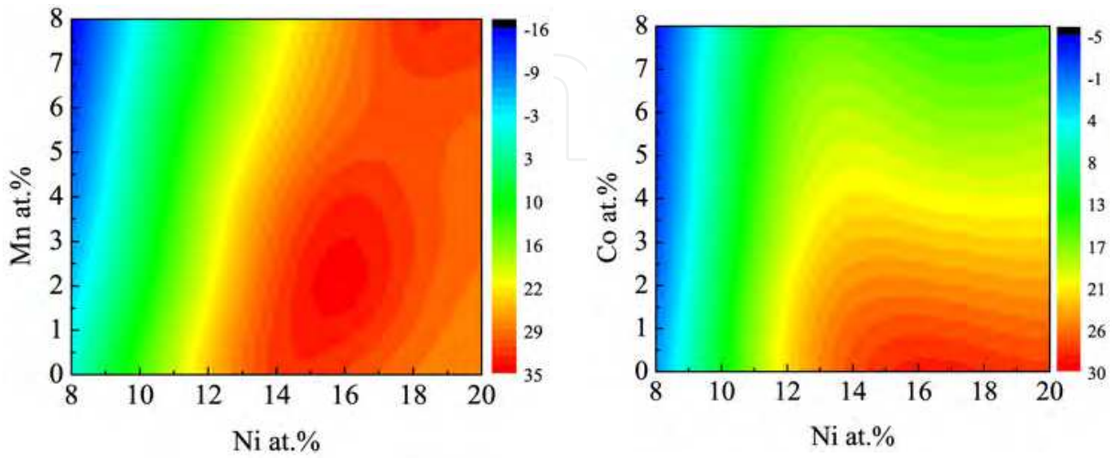

Fig. 10. Calculated stacking fault energy maps of Fe-Cr-Ni-Mn (left panel) and Fe-Cr-Ni-Co (right panel) alloys plotted as a function of composition for T = 300 K.

One important implication of the above finding is that the same alloying element can cause totally opposite changes in the SFE of alloys with different host composition, indicating that in practice no universal composition equations for the SFE can be established. To illustrate this effect, in Fig. 10 we show the theoretical room-temperature SFE maps for Fe-Cr-Ni-Mn and Fe-Cr-Ni-Co alloys as a function of composition (Lu et al., 2011). It is found that Mn decreases the SFE in alloys with less than 16 at.% Ni, beyond which the SFE slightly rises with Mn. On the other hand, Co always tends to decrease the SFE and the decreasing effect is enhanced in high-Ni alloys. Cobalt is known as a useful alloying element in improving the steel resistance against galling. Enhanced galling effect, in turn, is thought to be associated with enhanced ductility. According to our study (Fig. 10b), Co decreases the SFE and thus decreases the ductility of austenitic stainless steels. This might explain why Co acts as an efficient anti-galling alloying ingredient.

4.5 Surface properties

Stainless steels have versatile mechanical properties. However, the corrosion resistivity makes these materials unique among the engineering materials. For instance, the corrosion rate of ferritic stainless steels decreases drastically within a narrow concentration interval (9-13 wt. % Cr), (Khanna, 2002; Ryan et al., 2002; Wranglén, 1985) making the transition from iron type to non-corrosive behavior quite abrupt. The type of the oxide layer formed on the surface depends on the oxygen pressure, temperature and the alloy compositions in the vicinity of the surface. Further oxidation assumes transport of metal and oxygen ions through the initially formed oxide scale. The ion transport is controlled by diffusion, which in turn is determined by the defect structure of the oxide layer. The high mobility of Fe in Fe

oxides, especially in FeO, which is the dominant oxide component on pure iron above 570°C, explains the corrosive nature of Fe. The passivity in Fe-Cr, on the other hand, is attributed to a stable Cr-rich oxide scale. Above the critical concentration a pure chromia layer is formed on the surface which effectively blocks the ion diffusion across the oxide scale.

Kinetics of the thin layer oxidation and oxide scale formation have been explained using various models (Khanna, 2002). Numerous first-principles calculations have also focused on the properties of the Fe-rich Fe-Cr surfaces (Geng, 2003; Nonas et al., 1998; Ponomareva et al., 2007; Ruban et al., 1999). However, due to the involved approximations and constrains, most of these studies failed to reproduce the experimentally observed Cr enrichment on the alloy surface (Dowben et al., 1983). Later, using the exact muffin-tin orbitals method (Andersen et al., 1994; Vitos, 2001, 2007; Vitos et al., 2001) in combination with the generalized gradient approximation, it was demonstrated that the Fe-Cr surfaces exhibit a compositional threshold behavior (Ropo et al., 2007). In particular, it was shown that about 9 at. % chromium in Fe-Cr induces a sharp transition from Cr-free surfaces to Cr-containing surfaces. This surprising surface behavior was found to be a consequence of the complex bulk and surface magnetic interactions characteristic to the Fe-Cr system. The predicted surface chemical threshold has recently been confirmed by an independent theoretical study by Kiejna and Wachowicz (Kiejna & Wachowicz, 2008). Using the present achievements of the first-principles quantum mechanical approach many previously controversial results can now be merged into a consistent model of Fe-rich Fe-Cr alloys.

Before going into the details of the calculated surface properties we discuss some common procedures related to the first-principles surface calculations. The thermodynamically stable surfaces of the $Fe_{1-c}Cr_c$ alloys can be modeled by using periodic slab geometry consisting of a certain number of atomic layers, with surface alignment, joined to a set of empty layers representing the vacuum region. The thickness of the metal and vacuum regions is optimized keeping in mind both the computational cost on the one hand and the calculational accuracy on the other. In practice, the most common procedure in calculating the surface concentrations is to optimize the chemical composition of the surface layer only and to keep the concentrations of the other atomic layers fixed to the bulk value.

In magnetic systems, surface magnetism is observed to reduce the surface energy of open surfaces to the extent that the usual anisotropy of the surface energy is reversed (Aldén, Skriver, Mirbt, & Johansson, 1992, 1994; Vitos, Ruban, Skriver, & Kollár, 1998). In particular, the magnetic contribution to the surface energy of the (100) facet of pure Cr (Fe) is about -50% (-41%) compared to -2% (-16%) obtained for the close-packed (110) facet (Aldén et al. 1994). Accordingly, the most stable surfaces for pure Cr and for Fe-rich Fe-Cr alloys are the (100) crystal facet of the B2 lattice and the (100) crystal facet of the bcc lattice, respectively.

The atomic origin of the chemical threshold behavior of Fe-Cr surfaces (Ropo et al., 2007), becomes evident by considering the effective chemical potentials (ECPs) of the bulk and the (100) surface. Figure 11 (left axis) shows the bulk and surface ECP plotted as a function of the bulk Cr concentration. Data is shown for surfaces containing 0, 10, 20, and 30 at. % Cr. Comparing these curves one can easily construct a clear picture of the driving forces behind the peculiar trend of the surface chemistry of Fe-Cr alloys. At low Cr concentrations in bulk ($c < 0.08$), the ECP in bulk is above the ECP at the pure Fe surface. As a consequence, for

these alloys the Fe terminated surface is more favorable than the Cr containing surface. That is, Cr atoms are influenced by a large chemical driving force from the surface towards the bulk (Geng, 2003; Ropo et al., 2007). However, near 8 at. % Cr in the bulk alloy the ECP drops below the surface ECP leading to the transition from pure Fe terminated surfaces to Cr containing surfaces. The finding of the outburst of bulk Cr to the surface at about 9 at. % Cr in the bulk (Ropo et al., 2007) agrees well with the theoretical prediction based on Ising model (Ackland, 2009).

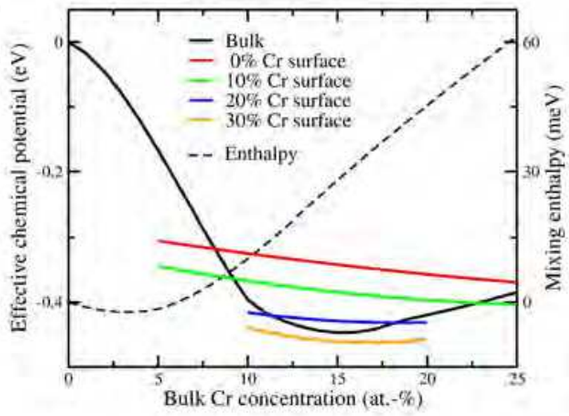

Fig. 11. Left axis (solid lines): Effective bulk (black) and surface (short coloured lines) chemical potentials (in eV) of ferromagnetic $Fe_{1-c}Cr_c$ alloys as a function of bulk Cr concentration (at. %) at T = 0 K. All curves are plotted relative to the bulk chemical potential for the dilute alloy. Left axis (dashed line): The mixing enthalpy (in meV) of disordered Fe-Cr alloy. The standard states are the ferromagnetic bcc Fe and antiferromagnetic B2 Cr. The inflection point in the mixing enthalpy around 15% Cr corresponds to the minimum of the bulk effective chemical potential (Ropo et al., 2007).

Figure 12 represents the calculated Cr concentration in the surface layer as a function of the Cr concentration in bulk, which describes well the characteristics of the experimentally observed compositional threshold (Wranglén, 1985). In particular, we emphasize that the calculated transition interval (8-12 % Cr) from Cr-free surfaces to surfaces with bulk-like composition is in excellent agreement with the concentration range within which the observed corrosion rate in Fe-Cr alloys drops from 0.1 mm per year near 9 % Cr to below the detectable limit at 13 % Cr (Wranglén, 1985). It should be noted that the sharp increase in the surface Cr content around the theoretical threshold in Fig. 12 can be traced back to the particular stability of pure Fe-terminated surfaces in low-Cr alloys rather than to a considerable surface segregation of Cr in high-Cr alloys.

In the following we analyze the data shown in Figs. 11 and 12 in more detail using the available theoretical data on bulk and surface Fe-Cr alloys. According to the surface segregation model (Ruban et al., 1999) of alloys with isostructural components the surface energy is an important driving force behind the segregation, namely, the alloy component with the lowest surface energy segregates toward the surface of the alloy. However, in Fe-Cr alloys the situation seems to be more complex. It turns out that, in spite of the large surface magnetic effects (Aldén et al., 1992, 1994; Vitos et al., 1998), the surface energy of pure Cr is significantly (~ 30%) larger than the one calculated for pure Fe (1.41 eV per surface Fe atom)

(Ropo et al., 2011; Ropo et al., 2007), thus preventing Cr atoms going to the surface. The surface energy difference between the pure Fe- and pure Cr-terminated surfaces is even larger (~36%) in Fe-rich Fe-Cr alloys. Thus, in contrast to Fig. 12 and experimental observations (Lince, Didziulis, Shuh, Durbin, & Yarmoff, 1992; Suzuki, Kosaka, Inone, Isshiki, & Waseda, 1996), from standard surface energy considerations the Cr-containing surfaces should always be energetically less favorable compared to the Cr-free surfaces. As a matter of fact, this contradictory picture is in line with several theoretical investigations carried out on diluted Fe-Cr alloys (Geng, 2003; Nonas et al., 1998; Ponomareva et al., 2007; Ruban et al., 1999).

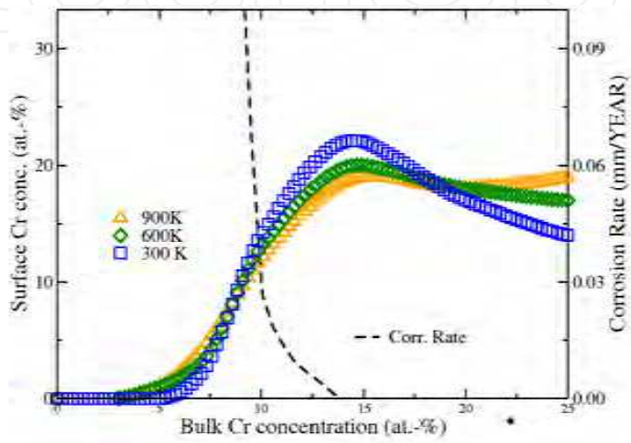

Fig. 12. The calculated Cr concentration in the surface layer (left axis) and the experimental corrosion rate (right axis), as a function of Cr concentration of bulk alloy in 300 K (blue square), 600 K (green diamond), and 900 K (yellow triangle).

The obvious failure of the surface energy considerations to explain the composition of the Fe-Cr surfaces indicates that the bulk part of the alloy could play a key role in the stability of Cr-containing surfaces. Bulk Fe-Cr alloys have a broad and slightly skewed miscibility gap, allowing the solubility of a small amount of Cr in Fe but not vice versa (Hultgren, Desai, Hawkins, Gleiser, & Kelley, 1973). The slightly negative mixing enthalpies at low Cr concentrations of the ferromagnetic solid solutions have been predicted theoretically (Klaver, Drautz, & Finnis, 2006; Olsson, Abrikosov, Vitos, & Wallenius, 2003; Olsson, Abrikosov, & Wallenius, 2006). It has been demonstrated (Ackland, 2006, 2009; Klaver et al., 2006; Nonas et al., 1998; Olsson et al., 2006; Olsson, Domain, & Wallenius, 2007) that the limited solubility of chromium in iron is connected to the complex magnetic interactions characteristic of solid solutions between antiferromagnetic (Cr) and ferromagnetic (Fe) species. These interactions originate from magnetic frustrations due to the strong antiparallel coupling between Cr and the Fe matrix and also between different Cr atoms (Nonas et al., 1998).

The energetically unfavorable magnetic interactions in Fe-Cr can be avoided or minimized by forming Cr-rich clusters (Klaver et al., 2006) and simultaneously moving some of the Cr atoms to the alloy surface. The latter phenomenon becomes clear if one compares the bulk ECP and the mixing enthalpy (Fig. 11). At low temperatures, apart from a constant shift and sign, the slope of the mixing enthalpy gives to a good approximation the value of the bulk

effective chemical potential (Nonas et al., 1998). Similarly, the second order concentration derivative (curvature) of the mixing enthalpy gives the slope of the bulk ECP. In particular, the large negative slope of the bulk ECP for Fe-Cr (Fig. 11, left axis) is related to the positive curvature of the mixing enthalpy of alloys with Cr content below ~ 15% (Fig. 11, right axis). When compared to the surface ECP, one can see that the crossover between the bulk and surface chemical potentials is indeed a consequence of the rapidly rising (convex) mixing enthalpy. On these grounds (Badini & Laurella, 2001; Götlind, Liu, Svensson, Halvarsson, & Johansson, 2007; Klaver et al., 2006), we can conclude that the magnetism-driven solubility of Cr in Fe is in fact the main factor responsible for the increasing stability of Cr containing surfaces compared to Fe-terminated surfaces (Ropo et al., 2011).

The decisive role of magnetic interactions in the bulk properties of Fe-Cr alloys has been proposed in several theoretical investigations (Ackland, 2006; Klaver et al., 2006; Nonas et al., 1998; Olsson et al., 2006; Olsson et al., 2007), but their impact on the surface chemical composition was revealed only recently. Figures 11 and 12, and the above arguments give clear evidence for the magnetic origin of the stability of Cr enriched surfaces for bulk concentrations beyond the (9%) threshold. It should be pointed out that the strongly nonlinear change of the surface Cr content versus bulk composition is due to the delicate balance between bulk and surface effects. In particular, the lack of Cr at the surface of Fe-rich alloys is a direct consequence of the anomalous mixing of Fe and Cr at low Cr concentrations, which in its turn has a magnetic origin. This finding has important implication in modern materials science as it offers additional rich perspectives in the optimization of high-performance steel grades.

To close our discussion of surface properties we consider an example where Cr enhances corrosion resistance indirectly. Chromium oxide gives good corrosion protection at usual operating temperatures but since Cr forms volatile compounds at high temperature the corrosion protection at elevated temperatures requires, for instance, the more stable Al oxide scales on the alloy surface. Cr_2O_3 scale is protective up to 1000-1100 °C whereas Al_2O_3 scales up to 1400 °C (Brady, Gleeson, & Wright, 2000; Ebbinghaus, 1993). Unfortunately, for most of the Fe alloy applications the straightforward procedure to improve high temperature corrosion resistance by increasing the Al content in bulk, is not an acceptable solution. This is because the high Al content makes Fe-Al alloys brittle which poses a natural upper bound for the Al content in these alloys regarding to most of the applications (Palm, 2005). Fortunately, the additional alloying of Fe-Al with Cr boosts the formation of the Al oxide scale on the surface up to such a level that the Al content in bulk can be kept within the acceptable limits regarding to the required mechanical properties of the alloy. This phenomenon, called the third element effect, is still considered a phenomenon without generally accepted explanation (Badini & Laurella, 2001; Götlind et al., 2007; Niu, Wang, Gao, Zhang, & Gesmundo, 2008; Stott, Wood, & Stringer, 1995; Z. G. Zhang, Gesmundo, Hou, & Niu, 2006). In Fig. 13 the calculated effective chemical potentials of Fe and Al ($\mu_{Fe} - \mu_{Al}$) in Fe-Cr-Al are shown as a function of Cr content. As Fig. 13 shows, Al surfaces are favoured in all cases, but Cr addition up to 10 at% decreases $\mu_{Fe} - \mu_{Al}$ in bulk whereas this quantity at the surface is almost constant. This builds up an increased driving force for the Al diffusion from bulk to the surface resulting in better corrosion resistance with less Al in bulk alloy.

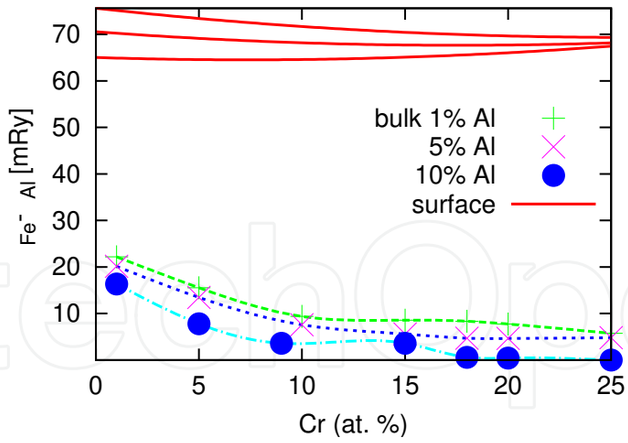

Fig. 13. Bulk and surface chemical potential differences ($\mu_{Fe} - \mu_{Al}$) of Fe-Cr-Al, (Al percentages for surface potentials from top to bottom: 1 at.%, 5 at.% and 10 at.%). Surface data is taken from two-dimensional polynomial fit and the calculated bulk values (shown by symbols) are connected by spline curves. The surface has the same composition as the bulk.

5. Conclusion

Magnetoelastic phenomena in magnetic materials and, in particular, in alloy steels have been known for a long time. However, the magnetic effects on the stacking fault energies and elastic constants of magnetic materials in their paramagnetic state have been less well documented. Here, using first-principles computational methods, we have investigated the atomic-scale chemical, magnetic and structural effects behind the elastic properties and stacking fault energies of paramagnetic Fe-Cr-Ni alloys. We have demonstrated that the presence of large disordered magnetic moments in the paramagnetic state can explain a wide diversity of properties that the austenitic stainless steels exhibit. Therefore, in this important class of „nonmagnetic" engineering materials, the „hidden" magnetism gives a major contribution to the fundamental bulk properties.

The interfacial energies between the Cr-rich Fe-Cr and Fe-rich Fe-Cr alloy phases have been calculated to be between ~0.02 and ~0.33 Jm^{-2} for the ferromagnetic state and between ~0.02 and ~0.27 Jm^{-2} for the paramagnetic state. The ferromagnetic interfacial energy exhibits strong nonlinear concentration dependence, whereas the paramagnetic interfacial energy follows smooth composition dependence. As an immediate application of the computed interfacial energies, we have estimated the critical grain size for phase separation using a continuum model. The theoretical critical radii depend very strongly on the composition of the initial homogeneous alloy. The rapidly increasing R_{crit} between the spinodal and solubility lines is in good agreement with the observation that in this region decomposition happens via the nucleation and growth mechanism. At a given volumetric driving force, it is the energy cost to form an interface which presents the main obstacle for decomposition. Therefore, shedding light on the atomic-level mechanisms behind the composition and magnetic state dependence of the interfacial energy opens perspectives for the quantum engineering of the Fe-Cr-based alloys. Our results present a step in this direction and give guidance for experimental and further theoretical investigations of the interfaces in Fe-Cr based alloys.

Investigating the surfaces of Fe-Cr alloys, we have demonstrated that the surface chemistry follows the peculiar threshold behavior characteristic of ferritic stainless steels. We find that in dilute alloys the surfaces are covered exclusively by Fe, whereas for bulk Cr concentration above ~10% the Cr-containing surfaces become favorable. The two distinctly dissimilar surface regimes appear as a consequence of two competing magnetic effects: the magnetically induced immiscibility in bulk Fe-Cr alloys and the stability of magnetic surfaces.

The above examples of *ab initio* study of steel materials have important message for modern materials science: they clearly show that a consistent approach to materials design must be based on first-principles quantum theory and thermodynamics. This combination offers a unique and probably the only possibility for a thorough control of the balance between competing atomic-level effects in steels.

6. Acknowledgment

The Swedish Research Council, the Swedish Steel Producers' Association (Jernkontoret), the Swedish Foundation for Strategic Research, the China Scholarship Council, the Erasmus Mundus External Cooperation Lot3, the Academy of Finland (Grant No. 116317) and Outokumpu Foundation and the Hungarian Academy of Sciences (research project OTKA 84078) are acknowledged for financial support.

7. References

Ackland, G. J. (2006). Magnetically Induced Immiscibility in the Ising Model of FeCr Stainless Steel. *Phys. Rev. Lett., 97*, 015502.

Ackland, G. J. (2009). Ordered sigma-type phase in the Ising model of Fe-Cr stainless steels. *Phys. Rev. B, 79*, 094202.

Airiskallio, E., Nurmi, E., Heinonen, M. H., Väyrynen, I. J., Kokko, K., Ropo, M., et al. (2010). High temperature oxidation of Fe-Al and Fe-Cr-Al alloys: The role of Cr as a chemically active element. *Corros. Sci. 52*, 3394.

Al-Zoubi, N., Johansson, B., Nilson, G., & Vitos, L. (2011). The Bain path of paramagnetic Fe-Cr based alloys. *J. Appl. Phys., 110*, 013708.

Aldén, M., Skriver, H. L., Mirbt, S., & Johansson, B. (1992). Calculated surface-energy anomaly in the 3d metals. *Phys. Rev. Lett., 69*, 2296.

Aldén, M., Skriver, H. L., Mirbt, S., & Johansson, B. (1994). Surface energy and magnetism of the 3d metals. *Surf. Sci., 315*, 157.

Andersen, O. K., Jepsen, O., & Krier, G. (1994). *Lectures on Methods of Electronic Structure Calculations*. edited by Kumar, V., Andersen, O. K., & Mookerjee, A. Singapore: World Scientific Publishing, pp. 63–124.

Argon, A. S., Backer, S., McClintock, F. A., et al., (1966). *Metallurgy and Materials*. Ontario: Addison-Wesley Publishing Company.

Badini, C., & Laurella, F. (2001). Oxidation of FeCrAl alloy: influence of temperature and atmosphere on scale growth rate and mechanism. *Surf. Coat. Techn., 135*, 291.

Bain, E. C. (1924). The nature of martensite. *Trans. Am. Inst. Min. Metal. Eng., 70*, 25.

Brady, M. P., Gleeson, B., & Wright, I. G. (2000). Alloy design strategies for promoting protective oxide-scale formation. *J. Min. Met. Mat. Soc., 52*, 16.

Dowben, P. A., Grunze, M., & Wright, D. (1983). Surface segregation of chromium in $Fe_{72}Cr_{28}$(110) crystal. *Surf. Sci., 134*, L524.

Ebbinghaus, B. B. (1993). Thermodynamics of gas-phase chromium species – the chromium oxides, the chromium oxyhydroxides, and volatility calculations in waste incineration processes. *Combustion and Flame, 93*, 119.

Fleischer, R. L. (1963). Substitutional solution hardening. *Acta Metall., 11*, 203.

Geng, W. T. (2003). Cr segregation at the Fe-Cr surface: A first-principles GGA investigation. *Phys. Rev. B, 68*, 233402.

Ghosh, G., & Olson, G. B. (2002). The isotropic shear modulus of multicomponent Fe-base solid solutions. *Acta Mater., 50*, 2655.

Gibbs, J. W. (1948). *Collected Works*. New Haven Yale University Press.

Götlind, H., Liu, F., Svensson, J.-E., Halvarsson, M., & Johansson, L.-G. (2007). The effect of water vapor on the initial stages of oxidation of the FeCrAl alloy Kanthal AF at 900 ^{o}C. *Oxid. Met., 67*, 251.

Grimvall, G. (1976). Polymorphism of metals 3. Theory of temperature-pressure phase diagram of iron. *Phys. Scr., 13*, 59.

Györffy, B. L. (1972). Coherent-Potential Approximation for a Nonoverlapping-Muffin-Tin-Potential Model of Random Substitutional Alloys. *Phys. Rev. B, 5*(6), 2382.

Györffy, B. L., Pindor, A. J., Stocks, G. M., Staunton, J., & Winter, H. (1985). A first-principles theory of ferromagnetic phase transitions in metals. *J. Phys. F: Met. Phys., 15*, 1337.

Heinonen, M. H., Kokko; K., Punkkinen M. P. J., Nurmi, E., Kollár, J., & Vitos, L. (2011). Initial oxidation of Fe-Al and Fe-Cr-Al Alloys: Cr as an alumina booster. *Oxid. Met. 76*, 331.

Hillert, M. (1961). A solid-solution model for inhomogeneous systems. *Acta Metall., 9*, 525.

Hohenberg, P., & Kohn, W. (1964). Inhomogeneous Electron Gas. *Phys. Rev. , 136*, B864.

Hultgren, R., Desai, P. D., Hawkins, D. T., Gleiser, M., & Kelley, K. K. (1973). *Selected Values of Thermodynamic Properties of Binary Alloys*. Metals Park OH.

Ishida, K. (1976). Direct estimation of stacking fault energy by thermodynamical analysis. *Phys. Stat. Sol. A, 36*, 717.

Khanna, A. S. (2002). *Introduction to High Temperature Oxidation and Corrosion*: ASM International, Materials Park OH.

Kiejna, A., & Wachowicz, E. (2008). Segregation of Cr impurities at bcc iron surfaces: First-principles calculations. *Phys. Rev. B, 78*, 113403.

Klaver, T. P. C., Drautz, R., & Finnis, M. W. (2006). Magnetism and thermodynamics of defect-free Fe-Cr alloys. *Phys. Rev. B, 74*, 094435.

Kollár, J., Vitos, L., & Skriver, H. L. (2000). *in Electronic Structure and Physical Properties of Solids: the Uses of the LMTO Method, Lectures Notes in Physics, .* Berlin: Springer-Verlag.

Labusch, R. (1972). Statistical theories of solid solution hardening. *Acta Metall., 20*, 917.

Lince, J. R., Didziulis, S. V., Shuh, D. K., Durbin, T. D., & Yarmoff, J. A. (1992). Interaction of O_2 with the $Fe_{0.84}Cr_{0.16}$(001) surface studied by photoelectron spectroscopy. *Surf. Sci., 277*, 43.

Lo, K. H., Shek, C. H., & Lai, J. K. L. (2009). Recent developments in stainless steels. *Mat. Sci. Eng. R, 65*, 39.

Lu, S., Hu, Q. M., Johansson, B., & Vitos, L. (2011). Stacking fault energies of Mn, Co and Nb alloyed austenitic stainless steels. *Acta Mater., 59*, 5728.

Lu, S., Hu, Q. M., Yang, R., Johansson, B., & Vitos, L. (2010). First-principles determination of the α-α' interfacial energy in Fe-Cr alloys. *Phys. Rev. B, 82*, 195103.

Lung, C. W., & March, N. H. (1999). *Mechanical properties of metals: atomistic and fractal continuum approaches*: World Scientific Publishing Co. Pte. Ltd.

Majumdar, A. K., & Blanckenhagen, P. v. (1984). Magnetic phase diagram of Fe_{80-x} Ni_xCr_{20} ($10 < x < 30$) alloys. *Phys. Rev., 29*, 4079.

Massalski, T. B. (1986). *Binary Alloy Phase Diagrams* (Vol. 1). Ohio: American Society for Metals, Metals park.

Nabarro, F. R. N. (1977). The theory of solution hardening. *Phil. Mag., 35*, 613.

Niu, Y., Wang, S., Gao, F., Zhang, Z. G., & Gesmundo, F. (2008). The nature of the third-element effect in the oxidation of Fe-xCr-3 at.% Al alloys in 1 atm O_2 at 1000 ºC. *Corros. Sci., 50*, 345.

Nonas, B., Wildberger, K., Zeller, R., Dederichs, P. H., & Gyorffy, B. L. (1998). Magnetic properties of 4d impurities on the (001) surfaces of nickel and iron. *Phys. Rev. B, 57*, 84.

Olsson, P., Abrikosov, I. A., Vitos, L., & Wallenius, J. (2003). Ab initio formation energies of Fe-Cr alloys. *J. Nucl. Mater., 321*, 84.

Olsson, P., Abrikosov, I. A., & Wallenius, J. (2006). Electronic origin of the anomalous stability of Fe-rich bcc Fe-Cr alloys. *Phys. Rev. B, 73*, 104416.

Olsson, P., Domain, C., & Wallenius, J. (2007). Ab initio study of Cr interactions with point defects in bcc Fe *Phys. Rev. B, 75*, 014110.

Palm, M. (2005). Concepts derived from phase diagram studies for the strengthening of Fe-Al-based alloys. *Intermetallics, 13*, 1286.

Perdew, J. P., Burke, K., & Ernzerhof, M. (1996). Generalized gradient approximation made simple. *Phys. Rev. Lett., 77*, 3865.

Ponomareva, A. V., Isaev, E. I., Skorodumova, N. V., Vekilov, Y. K., & Abrikosov, I. A. (2007). Surface segregation energy in bcc Fe-rich Fe-Cr alloys. *Phys. Rev. B, 75*, 245406.

Rhodes, C. G., & Thompson, A. W. (1977). Composition dependence of stacking-fault energy in austenitic stainless steels. *Metall. Trans. A, 8A*, 1901.

Ropo, M., Kokko, K., Airiskallio, E., Punkkinen, M. P. J., Hogmark, S., Kollár, J., et al. (2011). First-principles atomistic study of surfaces of Fe-rich Fe-Cr. *J. Phys.: Cond. Mat., 23*, 265004.

Ropo, M., Kokko, K., Punkkinen, M. P. J., Hogmark, S., Kollár, J., Johansson, B., et al. (2007). Theoretical evidence of the compositional threshold behavior of FeCr surfaces. *Phys. Rev. B, 76*, 220401.

Ruban, A. V., Skriver, H. L., & Nørskov, J. K. (1999). Surface segregation energies in transition-metal alloys. *Phys. Rev. B, 59*, 15990.

Ryan, M. P., Williams, D. E., Chater, R. J., Hutton, B. M., & McPhail, D. S. (2002). Why stainless steel corrodes. *Nature, 415*, 770.

Schramm, R. E., & Reed, R. P. (1975). Stacking-fault energies of 7 commercial austenitic stainless steels. *Metall. Trans. A, 6A*, 1345.

Soven, P. (1967). Coherent-Potential Model of Substitutional Disordered Alloys. *Phys. Rev., 156*, 809.

Speich, G. R., Schwoeble, A. J., & Leslie, W. C. (1972). Elastic constants of binary iron-base alloys. *Metall. Trans., 3*, 2031.

Stott, F. H., Wood, G. C., & Stringer, J. (1995). The influence of alloying elements on the development and maintenance of protective scales. *Oxid. Met., 44*, 113.

Suzuki, S., Kosaka, T., Inoue, H., Isshiki, M., & Waseda, Y. (1996). Effect of the surface segregation of chromium on oxidation of high-purity Fe-Cr alloys at room temperature. *Appl. Surf. Sci., 103*, 495.

Takeuchi, S. (1969). Solid-solution strenthending in single crystals of iron alloys. *J. Phys. Soc. Japan, 27*, 929.

Teklu, A., Ledbetter, H., Kim, S., Boatner, L. A., McGuire, M., & Keppens, V. (2004). Single-crystal elastic constants of Fe-15Ni-15Cr alloy. *Metall. Mater. Trans. A, 35*, 024415.

Vitos, L. (2001). Total-energy method based on the exact muffin-tin orbitals theory. *Phys. Rev. B, 64*, 014107.

Vitos, L. (2007). *The EMTO Method and Applications, in Computational Quantum Mechanicals for Materials Engineers* London: Springer-Verlag.

Vitos, L., Abrikosov, I. A., & Johansson, B. (2001). Anisotropic Lattice Distortions in Random Alloys from First-Principles Theory. *Phys. Rev. Lett., 87*, 156401.

Vitos, L., & Johansson, B. (2009). Large magnetoelastic effects in paramagnetic stainless steels from first principles. *Phys. Rev. B, 79*, 024415.

Vitos, L., Korzhavyi, P. A., & Johansson, B. (2002). Elastic property maps of austenitic stainless steels. *Phys. Rev. Lett., 88*, 155501.

Vitos, L., Korzhavyi, P. A., & Johansson, B. (2006). Evidence of large magneto-structural effects in austenitic stainless steels. *Phys. Rev. Lett., 96*, 117210.

Vitos, L., Korzhavyi, P. A., Nilsson, J.-O., & Johansson, B. (2008). Stacking fault energy and magnetism in austenitic stainless steels. *Phys. Scr., 77*, 065703

Vitos, L., Nilsson, J.-O., & Johansson, B. (2006). Alloying effects on the stacking fault energy in austenitic stainless steels from first-principles theory. *Acta Mater., 54*, 3821.

Vitos, L., Ruban, A. V., Skriver, H. L., & Kollár, J. (1998). The surface energy of metals. *Surf. Sci., 411*, 186.

Wranglén, G. (1985). *Introduction to Corrosion and Protection of Metals*. New York: Chapman and Hall.

Zhang, H. L., Johansson, B., & Vitos, L. (2009). Ab initio calculations of elastic properties of bcc Fe-Mg and Fe-Cr random alloys. *Phys. Rev. B, 79*, 224201.

Zhang, H. L., Punkkinen, M. P. J., Johansson, B., Hertzman, S., & Vitos, L. (2010a). Single-crystal elastic constants of ferromagnetic bcc Fe-based random alloys from first-principles theory. *Phys. Rev. B, 81*, 184105.

Zhang, H. L., Punkkinen, M. P. J., Johansson, B., & Vitos, L. (2010). Theoretical elastic moduli of ferromagnetic bcc Fe alloys. *J. Phys.: Cond. Mat. 22*, 275402.

Zhang, Z. G., Gesmundo, F., Hou, P. Y., & Niu, Y. (2006). Criteria for the formation of protective Al_2O_3 scales on Fe-Al and Fe-Cr-Al alloys. *Corros. Sci., 48*, 741.

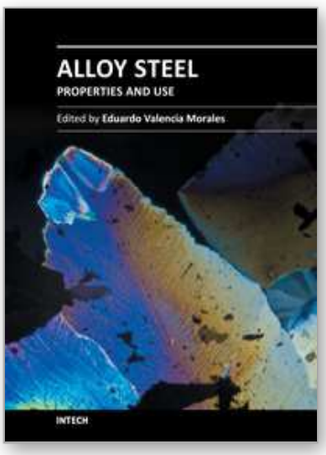

Alloy Steel - Properties and Use

Edited by Dr. Eduardo Valencia Morales

ISBN 978-953-307-484-9
Hard cover, 270 pages
Publisher InTech
Published online 22, December, 2011
Published in print edition December, 2011

The sections in this book are devoted to new approaches and usages of stainless steels, the influence of the environments on the behavior of certain classes of steels, new structural concepts to understand some fatigue processes, new insight on strengthening mechanisms, and toughness in microalloyed steels. The kinetics during tempering in low-alloy steels is also discussed through a new set-up that uses a modified Avrami formalism.

How to reference

In order to correctly reference this scholarly work, feel free to copy and paste the following:

L. Vitos, H.L. Zhang, S. Lu, N. Al-Zoubi, B. Johansson, E. Nurmi, M. Ropo, M. P. J. Punkkinen and K. Kokko (2011). Alloy Steel: Properties and Use First-Principles Quantum Mechanical Approach to Stainless Steel Alloys, Alloy Steel - Properties and Use, Dr. Eduardo Valencia Morales (Ed.), ISBN: 978-953-307-484-9, InTech, Available from: http://www.intechopen.com/books/alloy-steel-properties-and-use/alloy-steel-properties-and-use-first-principles-quantum-mechanical-approach-to-stainless-steel-alloy

INTECH
open science | open minds

InTech Europe
University Campus STeP Ri
Slavka Krautzeka 83/A
51000 Rijeka, Croatia
Phone: +385 (51) 770 447
Fax: +385 (51) 686 166
www.intechopen.com

InTech China
Unit 405, Office Block, Hotel Equatorial Shanghai
No.65, Yan An Road (West), Shanghai, 200040, China
中国上海市延安西路65号上海国际贵都大饭店办公楼405单元
Phone: +86-21-62489820
Fax: +86-21-62489821

IntechOpen